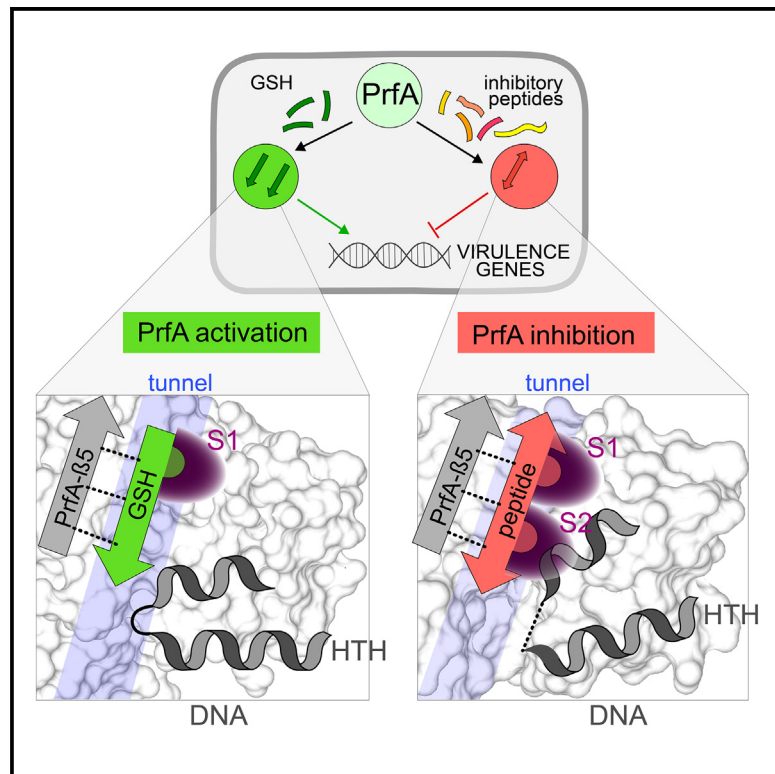


Structural basis of promiscuous inhibition of *Listeria* virulence activator PrfA by oligopeptides

Graphical abstract



Authors

Tobias Hainzl, Mariela Scotti,
Cecilia Lindgren, Christin Grundström,
Emilia Krypotou,
José A. Vázquez-Boland,
A. Elisabeth Sauer-Eriksson

Correspondence

v.boland@ed.ac.uk (J.A.V.-B.),
elisabeth.sauer-eriksson@umu.se
(A.E.S.-E.)

In brief

Hainzl et al. structurally explain the mechanism of promiscuous (sequence-independent) inhibition of *Listeria* virulence activator PrfA by environmental oligopeptides. Parallel and antiparallel β sheet-like interactions mediate nonspecific peptide docking at the binding site of the PrfA-activating cofactor, glutathione (GSH). Side-chain contacts afford inhibitory selectivity for peptides containing two adjacent hydrophobic residues.

Highlights

- Oligopeptides inhibit PrfA by blocking the binding tunnel for the activating cofactor GSH
- β Sheet-like interactions (parallel or antiparallel) mediate promiscuous peptide binding
- Two hydrophobic peptide residues contacting PrfA sites S1 and S2 modulate the interaction
- Oligopeptide binding prevents the proper positioning of the DNA-binding HTH motifs of PrfA



Article

Structural basis of promiscuous inhibition of *Listeria* virulence activator PrfA by oligopeptides

Tobias Hainzl,¹ Mariela Scotti,² Cecilia Lindgren,¹ Christin Grundström,¹ Emilia Kryptou,² José A. Vázquez-Boland,^{2,*} and A. Elisabeth Sauer-Eriksson^{1,3,*}

¹Department of Chemistry and Umeå Centre for Microbial Research, Umeå University, 901 87 Umeå, Sweden

²Microbial Pathogenomics Group, Edinburgh Medical School (Biomedical Sciences), Edinburgh BioQuarter, IRR Bldg. South, University of Edinburgh, Edinburgh EH16 4UU, UK

³Lead contact

*Correspondence: v.boland@ed.ac.uk (J.A.V.-B.), elisabeth.sauer-eriksson@umu.se (A.E.S.-E.)

<https://doi.org/10.1016/j.celrep.2025.115290>

SUMMARY

The facultative pathogen *Listeria monocytogenes* uses a master regulator, PrfA, to tightly control the fitness-costly expression of its virulence factors. We found that PrfA activity is repressed via competitive occupancy of the binding site for the PrfA-activating cofactor, glutathione, by exogenous nutritional oligopeptides. The inhibitory peptides show different sequence and physicochemical properties, but how such a wide variety of oligopeptides can bind PrfA was unclear. Using crystal structure analysis of PrfA complexed with inhibitory tri- and tetrapeptides, we show here that the binding promiscuity is due to the ability of PrfA β5 in the glutathione-binding inter-domain tunnel to establish parallel or antiparallel β sheet-like interactions with the peptide backbone. Spacious tunnel pockets provide additional flexibility for unspecific peptide accommodation while providing selectivity for hydrophobic residues. Hydrophobic contributions from two adjacent peptide residues appear to be critical for efficient PrfA inhibitory binding. In contrast to glutathione, peptide binding prevents the conformational change required for the correct positioning of the DNA-binding helix-turn-helix motifs of PrfA, effectively inhibiting virulence gene expression.

INTRODUCTION

Listeria monocytogenes, the causative bacterium of foodborne listeriosis, is an archetypal facultative pathogen that can live freely in the environment or parasitically within mammalian cells.^{1–3} Maintaining optimal fitness across this dual lifestyle is essential for the competitiveness and evolutionary viability of this type of pathogens. This is largely achieved by master regulators that turn virulence genes on during infection and switch off their expression outside the host.^{4–6} In *Listeria*, this role is fulfilled by the virulence regulator PrfA, a bacterial Crp/Fnr transcription factor.^{7–10} PrfA controls 10 key virulence genes, the so-called PrfA regulon,^{11,12} which are strongly induced intracellularly and repressed during saprophytic growth.^{5,13–15}

PrfA-dependent expression is modulated by signals that allow *L. monocytogenes* to sense the saprophyte-to-pathogen transition.^{13,14} For example, an RNA thermoswitch inhibits *prfA* gene translation at temperatures below 30°C, as would be found outside a warm-blooded host.¹⁶ PrfA-regulated genes are also repressed upon utilization of certain sugars, in particular plant-derived β-glucosides such as cellobiose,¹⁷ presumably abundant in the soil habitat of *L. monocytogenes*.¹⁸ Free fatty acids also interfere with the DNA-binding activity of PrfA.¹⁹ PrfA-dependent virulence gene expression, on the other

hand, is upregulated by a reducing environment,²⁰ or by stress signals and poor amino acid availability via the SigB and CodY regulators, respectively.^{21–23} To what extent the above PrfA-modulating cues and mechanisms contribute to the strong activation of listerial virulence genes observed in host cells remains uncharacterized.

A major step in understanding the listerial virulence gene “on-off” switching was the discovery that PrfA activity *in vivo* requires the redox tripeptide glutathione (γ -L-glutamyl-L-cysteinylglycine [GSH]).²⁴ In *L. monocytogenes*, GSH is endogenously synthesized by the glutathione synthase, GshF,²⁵ and an intact *gshF* gene in addition to PrfA is essential for virulence.^{20,24,26} PrfA is a dimeric protein of 54.5 kDa formed by two identical monomers, each comprising two distinct domains connected via an interfacial α -helix linker.^{27,28} The N-terminal domain is an eight-stranded cyclic nucleotide binding domain (CNBD) β sandwich of unknown function in PrfA. The C-terminal domain contains the DNA-binding helix-turn-helix (HTH) motif. Each of the two HTHs binds to one of the arms of the 14-bp palindromic sequence called the “PrfA-box” located at the –35 region of the target promoters.^{8,12,29} GSH binds to PrfA with low affinity ($K_D \approx 4$ mM),²⁴ in a large tunnel between the N- and C-terminal domains.³⁰ GSH binding to each PrfA monomer stabilizes the dimer in the active “on” conformation



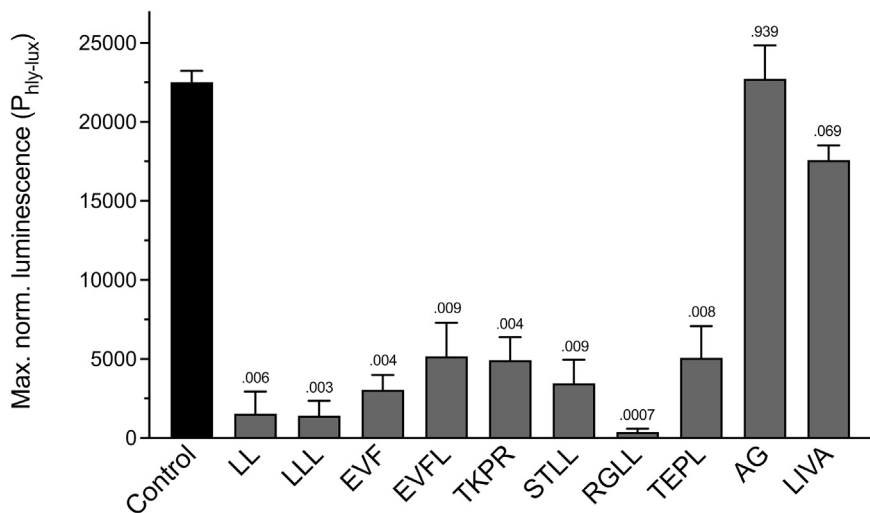


Figure 1. PrfA inhibitory activity of peptides

PrfA-dependent virulence gene expression of *L. monocytogenes* P14-P_{hly-lux} in chemically defined medium (CDM) without (control) or with 1 mM peptide. Quantified as maximum luminescence normalized to bacterial growth (optical density at 600 nm).²⁶ Mean values \pm SEM of three triplicate experiments. p values relative to control are indicated (one-way ANOVA and Dunnett's test for multiple comparisons). In the test conditions (CDM containing all amino acids required by *Listeria*), addition of the peptides did not affect bacterial growth (see Figure S1), ruling out that the observed PrfA-dependent gene expression inhibition was due to changes in the *L. monocytogenes* growth dynamics or to indirect metabolic effects.

with the HTH motifs correctly folded for productive interaction with the PrfA-box.³⁰

While GSH was identified as a critical PrfA-activating cofactor, it remained unclear how GSH-dependent PrfA activation was controlled. Recent studies identified a GSH-specific importer in *L. monocytogenes* that enables the direct transfer of GSH from the host cytoplasm.³¹ However, uptake of exogenous GSH alone is not sufficient for intrabacterial GSH concentrations to reach the threshold for normal PrfA activation; this requires endogenous GSH synthesis via the listerial GshF enzyme.^{20,24,26} Since *L. monocytogenes* is virtually auxotrophic to cysteine, GshF-mediated GSH biosynthesis requires uptake of this essential GSH precursor. Although free cysteine can be imported via the *L. monocytogenes* TcyKLMN ABC transporter,³² we showed that efficient GSH biosynthesis depends on the uptake of cysteine-containing peptides via the listerial Opp permease.²⁶ Furthermore, we also showed that the PrfA-GSH system is regulated by the composition of Opp-imported oligopeptides, as follows: peptides that provide cysteine (GSH precursor) activate PrfA; conversely, peptides lacking cysteine directly inhibit PrfA. Through this mechanism, *L. monocytogenes* exploits oligopeptides—an abundant and critical nitrogen source for microbial growth—to sense its habitat and control PrfA activity and virulence gene expression.²⁶

Co-crystallization with an example inhibitory peptide, leucyl-leucine (LL), revealed the dipeptide bound at the GSH-binding site in one of the PrfA monomers, in the same extended conformation as the GSH tripeptide. However, LL binding prevented the correct positioning of the PrfA C-terminal DNA-binding helices.²⁶ Interestingly, tested inhibitory oligopeptides ranged from di- to octapeptides, with different chemical properties including both negatively and positively charged residues as well as hydrophobic, polar, and aromatic residues.

To gain detailed insight into the molecular mechanisms of peptide-mediated inhibition of PrfA, in this study we determined and analyzed the crystal structures of sequence-diverse peptides in complex with PrfA. We found that the peptides bind at the GSH-binding site, also referred to as the inter-domain tunnel site, by forming parallel or antiparallel main-chain-main-chain in-

teractions with the CNBD β strand β 5. In addition, hydrophobic pockets at the tunnel site afford some degree of binding selectivity by interacting with hydrophobic or aromatic side chains of two consecutive peptide residues. Our findings provide structural insights into the unique ability of PrfA to accommodate a wide range of inhibitory oligopeptides with diverse amino acid sequence.

RESULTS

Biophysical analysis of interactions between PrfA and inhibitory peptides

A number of PrfA inhibitory peptides of various chemical properties were selected among those having the strongest effect *in vivo* in *L. monocytogenes* (Figure 1) using a screening test-bed based on a PrfA-regulated lux reporter system, as previously described²⁶ (see details in STAR Methods). To gain functional insight into the direct interaction between PrfA and the peptides, we investigated the binding thermodynamics using isothermal titration calorimetry (ITC). The results, shown in Figure S2, indicated that the peptides bind to PrfA with a negative enthalpy change. Analysis of the integrated heat peaks as a function of ligand-to-protein ratio showed that peptides LLL and LL have the strongest affinity, with dissociation constants (K_D s) in the low micromolar range, approximately 2 and 5 μ M, respectively. Peptides EVF and EVFL had K_D values of approximately 12 and 15 μ M, respectively, while peptides STLL and RGLL showed weaker binding with K_D values of approximately 28 and 90 μ M, respectively. The binding affinities of peptides TKPR and TEPL could not be quantified under our experimental conditions (see STAR Methods).

To analyze how peptide binding affects the DNA-binding properties of PrfA, we performed bio-layer interferometry (BLI) experiments. All PrfA-inhibitory peptides significantly inhibited DNA binding. Consistent with the ITC data, peptides LLL, LL, and EVF were found to be the strongest inhibitors, with peptides LLL and LL completely blocking DNA binding (Figure 2). Peptides AG and LIVA with no significant PrfA-inhibitory activity *in vivo* (Figure 1) were used as controls.

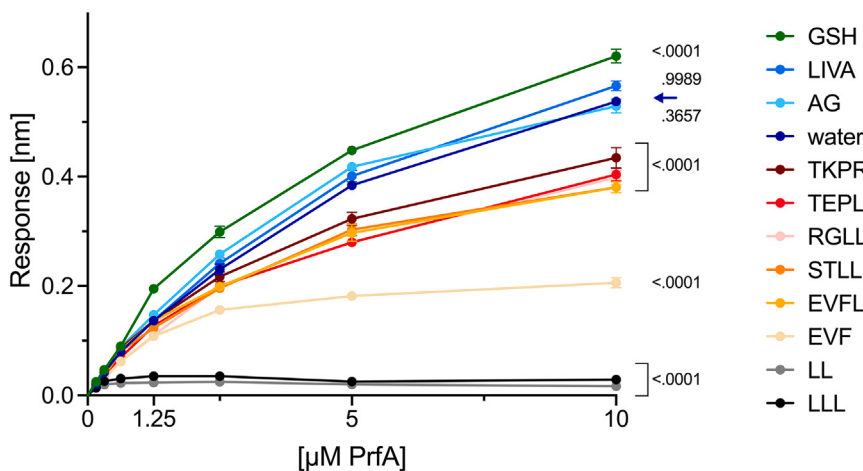


Figure 2. PrfA-DNA binding experiments

Inhibition of PrfA-DNA binding by oligopeptides as determined by bio-layer interferometry assays using PrfA-oligopeptide mixtures (1:100 M ratio) and the PrfA-box from the *PplcA/hly* promoter as target DNA. An equivalent volume of water mixed with PrfA was the control. For GSH, a concentration of 5 mM was used for all PrfA concentrations. Data are means \pm SEMs of triplicate experiments with corresponding *p* values of one-way ANOVA followed by Dunnett test for multiple comparisons. *p* values relative to control.

Inhibitory peptides bind to PrfA at the inter-domain tunnel

We determined the crystal structures of PrfA in complex with seven inhibitory peptides (LLL, EVF, EVFL, STLL, RGLL, TKPR, and TEPL; for data collection and refinement statistics see Table S1). Weak electron density for bound ligands due to conformational flexibility or low occupancy is a common problem in protein-ligand crystal structures. The use of bulk-solvent models in crystallographic refinement can also obscure densities in areas not occupied by protein atoms.³³ To overcome these limitations, in this study, we used polder maps³³ in addition to the classical difference maps. The LigandFit step in the procedure provided local correlation coefficient values over 0.75, which support binding of the peptide ligands to PrfA in all complexes studied (Table S2). Figure 3A illustrates the improvement in interpretability using the polder map of the tripeptide LLL as an example. The polder maps for the remaining peptides are shown in Figure S3.

PrfA is a 237-residue protein in which residues Met1-Asn109 and Gly138-Asn237 constitute the N- and C-terminal domains, respectively, connected by the linker helix spanning residues Leu110-Asn137. Our previous studies showed that the binding site for the GSH cofactor³⁰ and the dipeptide LL²⁶ is positioned at the inter-domain tunnel formed between the N- and C-terminal domains of the PrfA monomers. Although not all amino acids of the different peptides could be modeled (discussed below), all peptides in this study bound at this site. As an example, Figures 3B and 3C show the structure of the PrfA-LLL complex with the tripeptide bound to the tunnel site of monomers A and B, respectively. All other peptides also bind to the tunnel site in monomers A and B, with the exception of TEPL. This tetrapeptide was found only in monomer A, as was the previously studied LL dipeptide. This may reflect negative cooperativity in the binding of peptides to the PrfA dimer, where the binding of a ligand to one monomer affects the shape of the other monomer such that the binding affinity of the ligand decreases. Such negative cooperativity was observed in previous studies of PrfA in complex with 2-pyridone PrfA inhibitors.^{34,35}

In the previous structure-guided 2-pyridone inhibitor studies, two binding pockets at the tunnel site, S1 and S2, were predicted

to allow for some degree of selectivity in the PrfA-ligand interaction.³⁵ Selectivity pocket S1 creates possibilities for hydrophobic interactions with the side chains

of PrfA residues Tyr63, Phe67, Tyr126, and Trp224; pocket S2 does the same for Ile45, Tyr62, Ile149, Leu150, Tyr154, and Leu174. All PrfA-inhibitory peptides studied here had hydrophobic side chains that bound to the S1 and S2 pockets. The same was reported for the binding of the dipeptide LL to PrfA, confirming the functional importance of the inter-domain tunnel S1 and S2 pockets in the PrfA-peptide interaction (Figures 3D and 3E).

Interaction in parallel or antiparallel β sheet-like conformations underpins peptide binding flexibility

Except for TKPR, all peptides in this study are in an extended β strand-like conformation: they establish main-chain contacts with PrfA strand β 5 (Gln61-Lys64) and the turn leading to β 6 (Gly65-Phe67) (Figure S4). A close-up view of PrfA β 5 shows that it can form five main-chain hydrogen bonds with an incoming peptide (Figure 4A). In addition, due to the *cis*-peptide bond between residues Gly65-Ala66, there are possibilities for hydrogen bonding with the main-chain carbonyl oxygen of Ala66. Five of the peptides—EVF, EVFL, LLL, STLL, and TEPL—bind antiparallel to β 5 by forming 3 to 5 main-chain hydrogen bonds (Figures 4B, 4C, and S4). The polder maps showed that the first residue in both STLL and TEPL is flexible and could not be modeled; thus, the modeled β 5-binding residues for these peptides are -TLL and -EPL, respectively. EVFL, which is a 1-amino acid extension of EVF, binds its first three residues identically to those of the tripeptide. In addition, the main-chain nitrogen atom of Leu4 in EVFL makes a hydrogen bond to the side chain of Gln146, and its side chain packs against that of Leu174 (Figure S4D). Despite these additional hydrogen bonds, the EVFL peptide binds to PrfA with lower affinity than EVF. We can only speculate that this is due to the position of the carboxyl group of the EVFL peptide, which causes a rotamer switch of Glu146 and is located in an hydrophobic part of the tunnel.

Interestingly, while the Leu dipeptide bound parallel to β 5 in the previous PrfA-LL crystal structure (PDB: 6hck), in the PrfA-LLL complex, the Leu tripeptide binds in an antiparallel conformation (Figure 4C). The side chains of the second and third leucine in the tripeptide bind identically to the Leu side chains of the

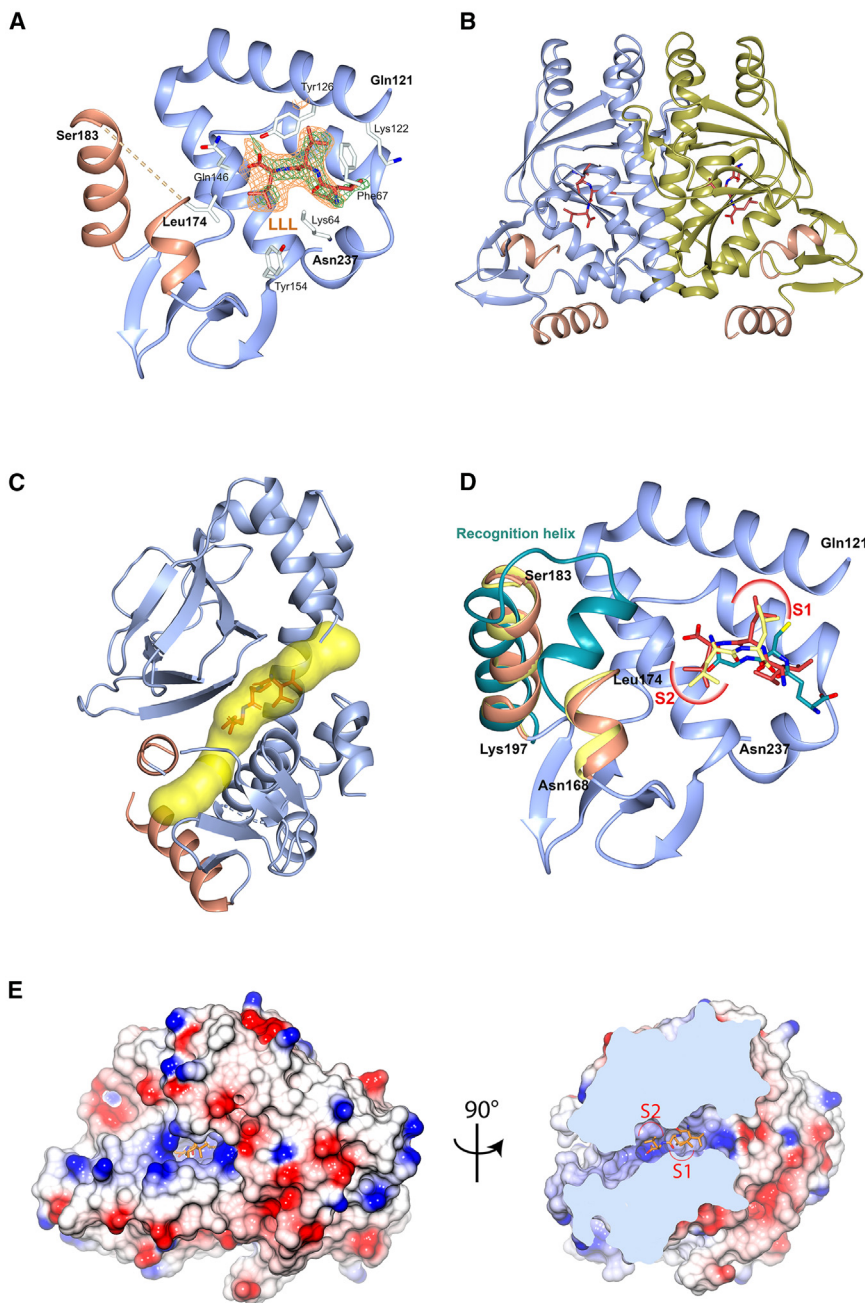


Figure 3. Oligopeptides bind to the inter-domain tunnel of PrfA

(A) Ribbon representation of the C-terminal domain of monomer A of the PrfA-LLL complex. Residues Gln121-Asn237 are shown in blue, with the HTH motif (residues Asn168-Lys197) highlighted in orange. For clarity, only the side chains of a few selected residues are shown as sticks. The LLL peptide is shown in crimson red. The first leucine residue of the peptide has two conformations. The difference ($|F_O - |F_C|$) and polder electron density maps are green and orange, respectively. The maps are contoured at three times the root-mean-square deviation value of the map, covering the LLL peptide only.

(B) Ribbon representation of the PrfA homodimer in complex with LLL. Monomers A and B are shown in blue and gold, respectively, the HTH motif is highlighted in orange, and the LLL peptide is crimson red.

(C) Structure of the PrfA-LLL complex showing a PrfA monomer with the main tunnel as a yellow surface.

(D) The figure outlines the position of the hydrophobic pockets S1 and S2 at the tunnel site of the PrfA-LLL complex. For clarity, no protein residues are shown. Superimposed are the structures of PrfA bound to LL (yellow; PDB: 6hck²⁶) and PrfA bound to the activator molecule GSH (dark cyan; PDB: 5lr³⁰).

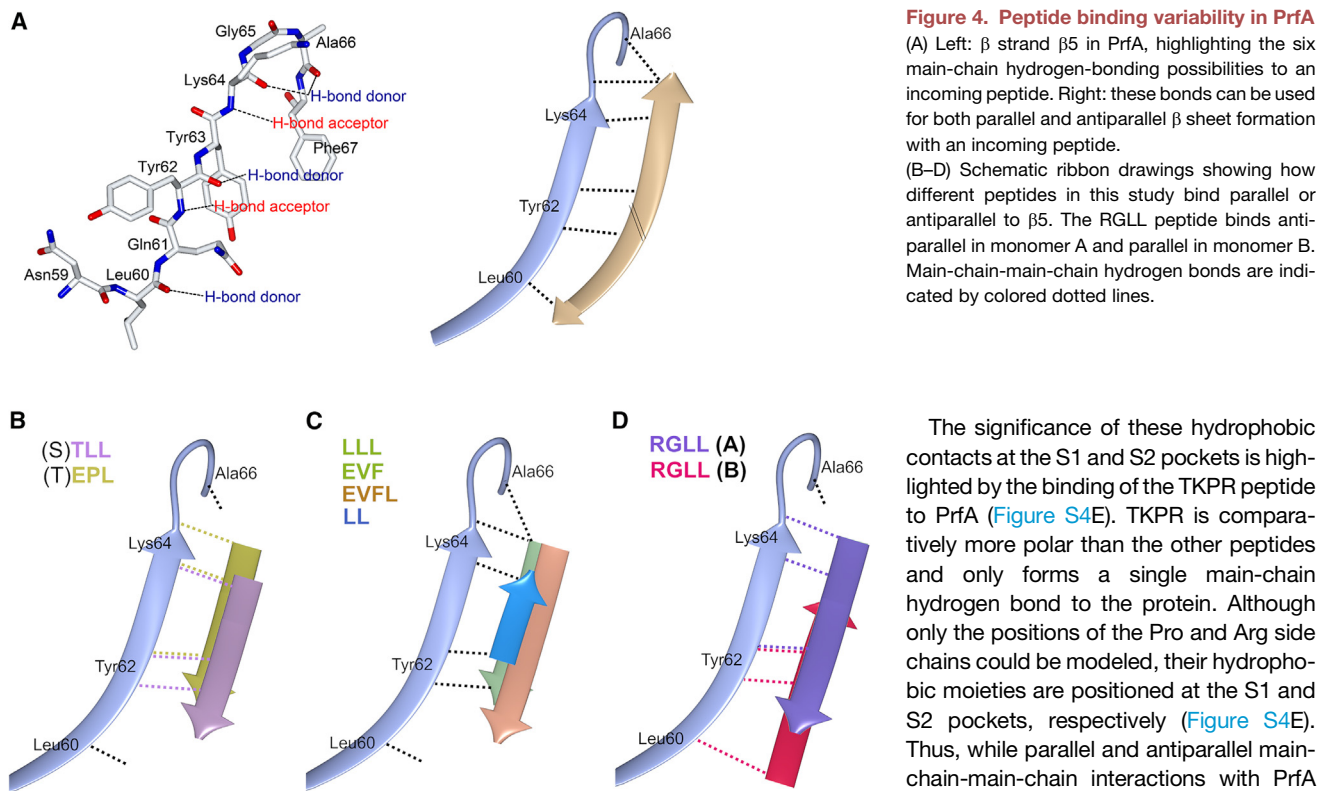
(E) Surface representation of the electrostatic charge distribution of $\pm 5 \text{ kT/e}$ of the PrfA dimer, with LLL bound at the tunnel site of monomer A. The figure shows two orientations rotated by 90°.

dipeptide at sites S1 and S2. Both peptides form two hydrogen bonds each to the main-chain carbonyl oxygen and amide nitrogen atoms of Tyr62 and Lys64, respectively (Figures S4A and S4I). In addition, the N-terminal nitrogen atom of LL forms a hydrogen bond to the hydroxyl group of Tyr126. The C-terminal carboxyl group of LLL, in turn, forms hydrogen bonds with the main-chain nitrogen atom and the Ne2 atom of Gln61. The only obvious structural difference between how LL and LLL bind to PrfA is the rotamer of Gln146 positioned in the vicinity of the HTH motif; it is closer, making an electrostatic interaction with the N-terminal amino group of the peptide in the PrfA-LL complex (Figure S4I). In

the PrfA-LLL structure, the side chain of Gln146 is positioned more than 4 Å away from the peptide (Figure S4A).

Strikingly, the RGLL peptide binds in both directions within the same dimer—antiparallel to β 5 in monomer A and parallel to β 5 in monomer B (Figure 4D). In both monomers, only the last two leucine residues of the tetrapeptide are well defined in the electron density (Figures S3G and S3H). In the antiparallel arrangement, the hydrogen bonding pattern to PrfA β 5 is similar to that of the tripeptides (e.g., LLL, EVF).

However, the C-terminal carboxyl group does not make a hydrogen bond with the main-chain nitrogen atom of Tyr62, but forms hydrogen bonds with the side chains of Gln61, Tyr126, and Gln146 (Figure S4G). In monomer B, the parallel binding of the peptide is made possible by hydrogen bonding with the main-chain oxygen atom of Gln61, the nitrogen and oxygen atoms of Tyr62, and the nitrogen atom of Lys64. In addition, there are interactions between the carbonyl oxygen of Arg1 of the peptide and the side chains of Lys130, and between the guanidinium group of Arg1 and the hydroxyl group of Ser142 (Figure S4H).



Thus, the two binding modes of the LL and LLL peptides and, in particular, of the tetrapeptide RGLL in the same dimer, highlight that slightly alternating hydrogen bonding to the PrfA protein can accommodate similar or even the same peptides in two different orientations, parallel and antiparallel to β 5.

In general, for all inhibitory peptides, the hydrogen bonds and van der Waal interactions formed between the peptide residues and PrfA residues Gln61, Tyr126, Gln146, and Leu174 prevent the conformational changes associated with PrfA activation and DNA binding.³⁰ This point is discussed later in the paper.

Hydrophobic motifs at the PrfA tunnel site contribute to inhibitory peptide binding

Superimposition of monomer A of the PrfA-LL and PrfA-LLL complexes shows that, in addition to main-chain β strand formation, the binding involves interactions between the hydrophobic side chains of two consecutive residues of the peptide and the S1 and S2 pockets within the inter-domain tunnel (Figure 5A). When all PrfA-peptide structures (including monomer B of the PrfA-RGLL complex) were superimposed, it became apparent that the additional contacts with the S1 and S2 sites are a general feature of the binding mechanism (Figure 5B). The side chains of the peptide residues Leu, Val, and Pro bound at the S1 site, making van der Waals interactions with the side chains of the aromatic residues Tyr63, Phe67, Tyr126, and Trp224. At the S2 site, the side chains of peptide residues Leu and Phe and the hydrophobic part of Arg made van der Waals interactions with the side chains of Ile45, Tyr62, Gln146, Ile149, Leu150, Tyr154, and Leu174 (Figure 5B).

The significance of these hydrophobic contacts at the S1 and S2 pockets is highlighted by the binding of the TKPR peptide to PrfA (Figure S4E). TKPR is comparatively more polar than the other peptides and only forms a single main-chain hydrogen bond to the protein. Although only the positions of the Pro and Arg side chains could be modeled, their hydrophobic moieties are positioned at the S1 and S2 pockets, respectively (Figure S4E). Thus, while parallel and antiparallel main-chain-main-chain interactions with PrfA β 5 enable flexible, sequence-independent peptide binding, a degree of binding

selectivity is ensured by two adjacent peptide residues that are able to establish hydrophobic contacts with the S1 and S2 pockets at the PrfA inter-domain tunnel. The main-chain atoms of these two hydrophobic residues make hydrogen bonds to the main-chain atoms of Tyr62 and Lys64 positioned at PrfA β 5. Their flanking residues are then positioned so that they make further contacts with PrfA via hydrogen bonds to the main-chain atoms of Leu60 and Gly65 or to the side chains of Gln61, Lys122, Tyr126, Lys130, and Gln146.

Some peptide residues could not be modeled due to poor electron density. The first serine and threonine residues of the peptides STLL and TEPL, respectively, are flexible and were not modeled (Figures S4C and S4F). These small and polar residues are situated in a hydrophobic part of the tunnel, lined by residues Phe67, Trp224, Phe225, and Cys229, with no hydrogen-bonding partner in the vicinity. For an inhibitory peptide, a hydrophobic residue such as leucine seems to be optimal, as can be seen in the LLL tripeptide. A glutamic acid directly preceding the hydrophobic residues bound in sites S1 and S2 is also favorable, as it can make electrostatic interactions with the side chains of Lys64 and Lys122, as seen in the EVF- and EVFL-bound structures (Figures S4B and S4D). However, since the glutamic acid in the TEPL peptide is poorly defined in the electron density, the interactions with the lysine residues are influenced by residues that precede the glutamic acid in the peptide (Figure S4F). The presence of Lys64 and Lys122 in this area also provides a structural explanation for why the first two residues, threonine and lysine, are flexible in the TKPR peptide (Figure S4E).

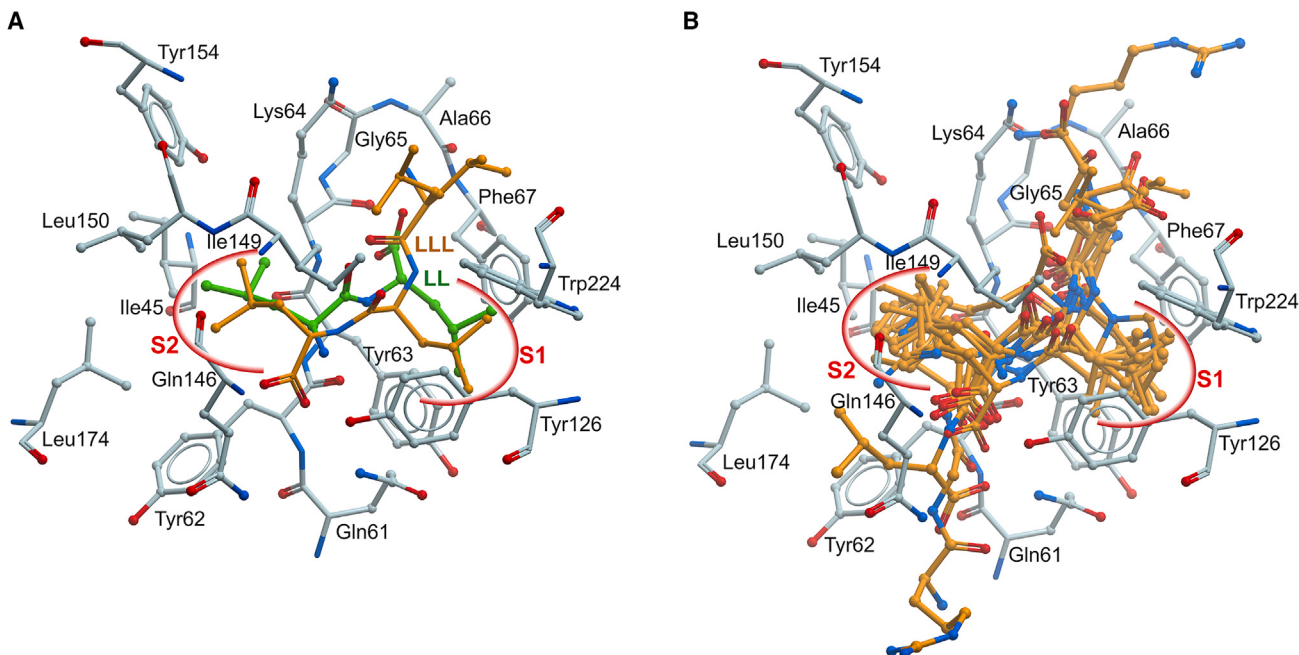


Figure 5. Peptide binding selectivity in PrfA

(A) Two consecutive leucine residues of the peptides LL (green) and LLL (orange) bind at the S1 and S2 sites of the protein, which provide selectivity to the binding. (B) Superimposition of all PrfA-peptide complexes highlights that hydrophobic residues bound at the S1 and S2 sites are a common feature of peptide binding to PrfA. All peptides, including LL, are shown in orange. For clarity, not all PrfA residues involved in peptide-binding interactions are shown.

GSH and the inhibitory peptides differ in their binding to PrfA

The PrfA-activating cofactor GSH binds at the inter-domain tunnel site of PrfA, where it forms β strand interactions with $\beta 5^{30}$ in a similar manner to the inhibitory peptides. However, even though the binding sites of the inhibitory peptides and the GSH activator overlap, the superimposition of the structures reveals several fundamental differences that explain their different effects on PrfA activity. First, GSH is not a true peptide, but a peptide-like molecule—a tripeptide with a gamma peptide linkage between the carboxyl group of the glutamate side chain and cysteine. As a consequence, the distance between the N-terminal nitrogen and oxygen atoms of the gamma peptide linkage in GSH is 4.8 Å, whereas in a regular peptide such as EVF, it is 2.7 Å (Figures 6A and 6B). This longer distance allows GSH to form more favorable hydrogen bond distances and angles to the main-chain oxygen atoms of Lys64 and Ala66 without disrupting the hydrogen bonding pattern to the rest of $\beta 5$ (Figure 6B). Second, GSH binding allows a structural movement of the C-terminal domain that closes the tunnel site and enables the formation of an active HTH motif. This movement positions critical amino acids (i.e., Gln146, Tyr154, and Leu174) in the vicinity of the HTH motif in the PrfA-GSH complex. In their new positions, these residues bridge the bound GSH molecule and the HTH motif, allowing a network of water molecules to connect the C-terminal carboxyl group of GSH to the HTH motif, which is now properly folded and compatible with DNA binding.³⁰ In other words, the unique set of interactions of GSH within each inter-domain tunnel of the PrfA dimer leads to the

correct positioning of the PrfA DNA-binding helices from each monomer, as required for PrfA productively interacting with the dyad symmetric target DNA sequence, with no additional changes to the PrfA-GSH structure occurring when bound to DNA^{12,30} (Figure S5A).

Specifically, the position of the glycine residue of GSH at site S2 appears to be crucial for the activation of PrfA (Figure 6B). This is because only glycine, lacking a side chain, can accommodate the bulky side chain of the incoming Tyr154 residue in the PrfA-GSH structure.³⁰ In contrast, the bound inhibitory peptides block the collapse of the tunnel by interacting with residues such as Tyr126, Gln146, and Leu174. Furthermore, with their hydrophobic side chains positioned at S2 (Figure 5B), the inhibitory peptides sterically prevent activating conformational changes of the C-terminal domain, exemplified here by the tunnel-closing movement of residue Tyr154 (Figures 6C, 6D, and S5B–S5D).

DISCUSSION

Protein-peptide interactions are ubiquitous in biological systems and mediate key cellular processes such as signaling and regulation, protein trafficking, DNA repair, or immune recognition.^{36–38} Here, we report the structural basis of a protein-peptide interaction that controls the activity of a transcriptional activator, PrfA, the master regulator of *Listeria* virulence.¹³ The interacting peptides are small nutritional oligopeptides of different sequence and physicochemical properties scavenged from the medium via the listerial Opp transporter.²⁶ In this study,

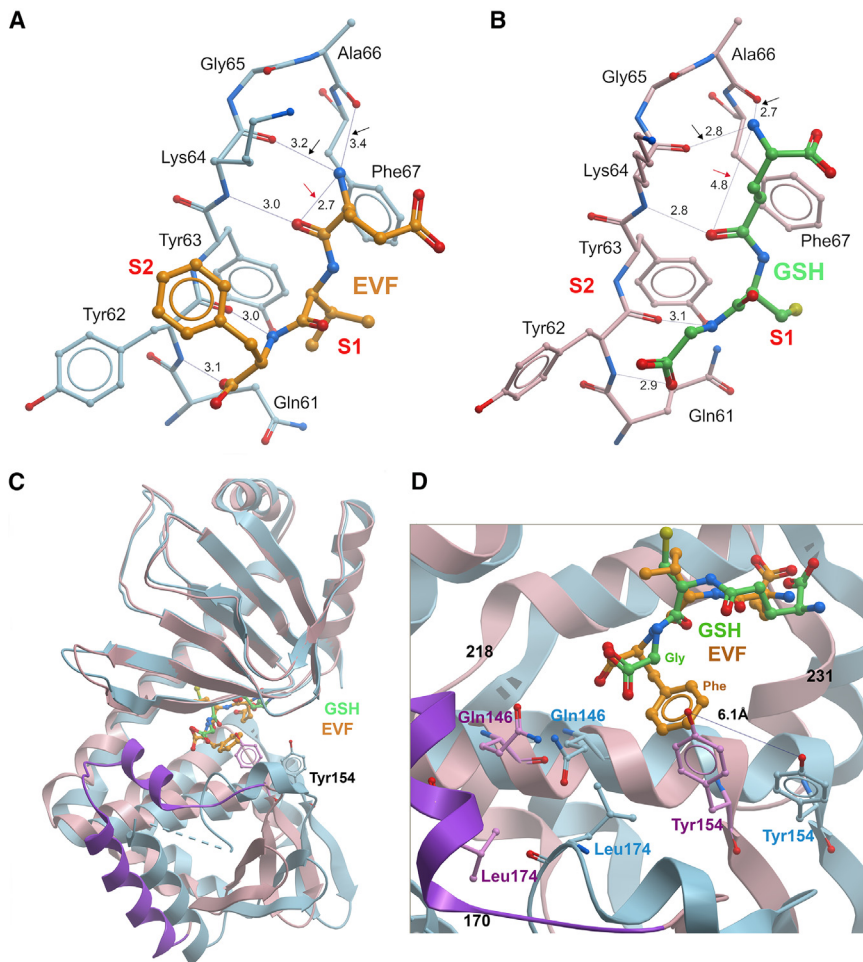


Figure 6. Differences in the binding of the inhibitor peptide EVF and the activator GSH molecule to PrfA

(A) Binding of peptide EVF.
 (B) Binding of GSH. The distance between the main-chain nitrogen and oxygen atoms in the gamma peptide linkage in GSH is 2 Å longer than the same distance in a regular peptide (4.8 Å in GSH compared to 2.7 Å in EVF, red arrows). This enables GSH to make hydrogen bonds to the main-chain carbonyl oxygens of Lys64 and Ala66 of β5 with favorable bonding distances and angles (black arrows). Furthermore, GSH has no hydrophobic side chain bound at S2, a common feature of all inhibitory peptides. In EVF, the side chain of Phe3 is positioned at S2. Structural coordinates for the PrfA-GSH complex are from PDB: 5lr.³⁰
 (C) Superimposition of monomer A of EVF-inhibited (blue) and GSH-activated (pink) PrfA based on residues Asn2-Gln123 in the N-terminal domain. Residue Tyr154, which exemplifies the large GSH-induced structural movement of the C-terminal DNA-binding domain, is shown as ball-and-sticks representations in both structures.
 (D) Close-up view of the ligand binding site in (C), highlighting the closing in of the C-terminal domain of PrfA toward the GSH cofactor at the tunnel site. Also highlighted is the steric clash between the Phe3 side chain of the EVF inhibitor peptide and the Tyr154 side chain in the GSH-activated structure (pink). The same steric clash occurs for all inhibitory peptides with hydrophobic side chains positioned at site S2 (Figure 5B).

the mechanism of promiscuous binding of these peptides to PrfA was characterized.

The structural analyses of the PrfA-peptide interactions show that the binding mechanism involves a combination of variability and selectivity. Variability is provided by nonspecific main-chain-main-chain interactions (β sheet-like), whereas selectivity relies on hydrophobic contacts at two selectivity sites, S1 and S2,^{36–38} in the PrfA inter-domain tunnel. In the peptides tested, these interactions involve residues Leu, Val, and Pro at the S1 site, and Leu, Phe, and the aliphatic side chain of Arg, at the S2 site. Based on our observations, we suggest that two consecutive hydrophobic residues of the peptide binding to the S1 and S2 sites are important for defining the binding affinity to PrfA. Furthermore, the PrfA-TEPL structure showed binding of the tetrapeptide only to monomer A. This feature was also observed in the previously studied PrfA-LL dipeptide structure²⁶ and in PrfA structures in complex with 2-pyridone inhibitors.³⁴ From our analyses, we cannot derive a structural explanation for the observed binding discrepancies in monomers A and B. However, a similar effect was reported for the Crp/Fnr transcription factors CAP from *Escherichia coli* and GlxR from *Corynebacterium glutamicum*, where binding of the first molecule of the cyclic AMP (cAMP) ligand was correlated

with negative cooperativity for binding of the second cAMP ligand without a conformational change.³⁹

The results of our biophysical analyses supported the structural data, confirming that the direct interaction between the inhibitory peptides and PrfA results in impaired DNA-binding activity (Figures 2 and S2). There was a general correlation between the effect of the peptides on PrfA-DNA binding and the observed *in vivo* effects on virulence gene expression in the bacterial system. Only one of the peptides, RGLL, showed a relatively weaker effect on DNA binding but had a strong virulence gene expression-inhibitory activity (Figures 1 and 2). This could be due to experimental variation, an additional unknown effect of this particular peptide on virulence gene expression, or simply reflect delayed proteolytic processing increasing the half-life of the peptide in *L. monocytogenes*. Importantly, when bound to PrfA, as observed in our crystal structures, all investigated inhibitory peptides sterically prevent the collapse of the tunnel that is required for the formation of the activated structure of PrfA.³⁰

PrfA-peptide binding bears some of the general features of protein-peptide interactions, reinforcing the notion that common principles underlie the binding of intrinsically flexible peptide ligands to proteins.³⁸ These include preferential binding in β strand/β strand-like conformation; binding involving hydrogen bonds with the peptide backbone; and binding also generally

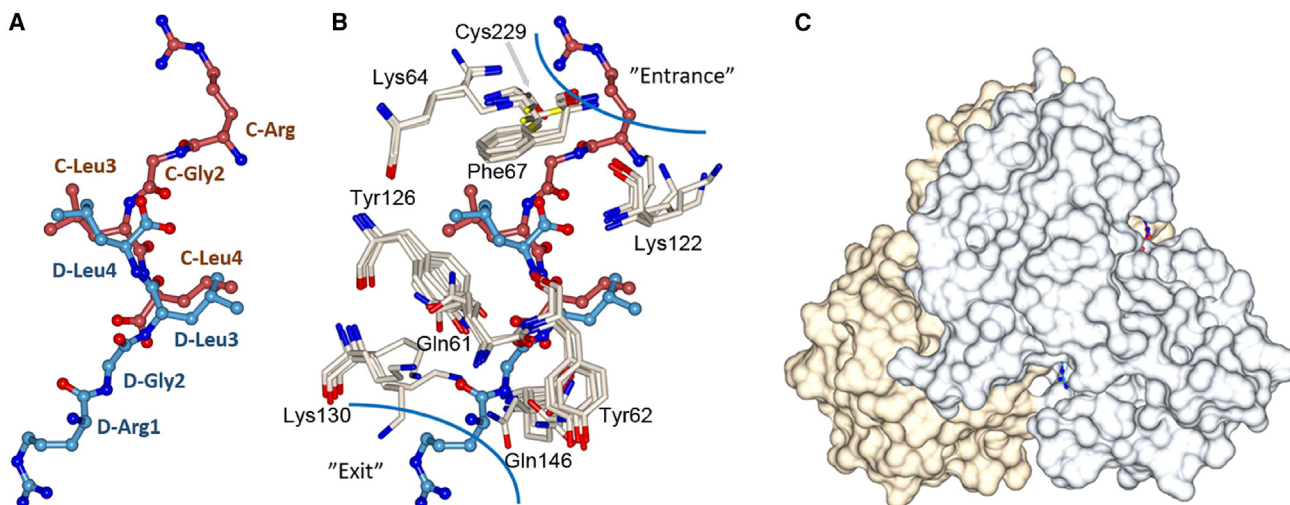


Figure 7. Gatekeeper residues at the PrfA tunnel site

(A) Superimposition of monomers A and B in the PrfA-RGLL complex assembles the parallel- and antiparallel-bound RGLL peptides into a virtual RGLLGR peptide. The figure shows C-RGLL (red) and D-RGLL (blue) bound in monomers A and B, respectively. Combined, the peptides span six residues.

(B) Gatekeeper residues (i.e., Tyr62, Lys122, Lys 130, and Gln146) can change their rotamers to accommodate variable peptide side chains at the entrance and exit of the tunnel. For clarity, only the residues of PrfA bound to LLL in monomer A, EVF in monomer A, and RGLL in monomers A and B are shown.

(C) The length and position of the artificial RGLLGR peptide suggests that in hexapeptides, for example, the first and last residues protrude from the tunnel site when residues 3 and 4 are hydrophobic and bind at sites S1 and S2.

relying on hotspot or anchor residues in the peptide, with a predominance of hydrophobic leucine and aromatic residues^{36–38,40–42}, as also seen in our case.

Peptide-mediated PrfA inhibition by competitive occupancy of the tunnel binding site for GSH, itself a tripeptide, could be attributed to rapid, transient protein-peptide interactions with relatively weak affinity, like those that dynamically regulate cellular processes via short linear motifs (SLiMs).⁴³ Indeed, the K_D values for the PrfA-inhibitory peptide complexes were determined with ITC to be between 2 and 90 μM (Figure S2). These values are in the range of those determined for SLiMs and their protein targets (K_D of 1–500 μM), in contrast to the nanomolar range typical of highly specific ligand-receptor interactions.⁴³ However, whereas peptide and SLiMs-protein interactions are mostly specific,^{38,43,44} a salient feature of the peptide-mediated PrfA inhibition is its promiscuity.²⁶ Our study shows that likely major determinants of this binding promiscuity are (i) the unique ability of the inhibitory peptides to interact with PrfA β 5 in both parallel and antiparallel conformations, and (ii) the non-specific accommodation of hydrophobic and aromatic residues of the peptide in the spacious pockets within the PrfA inter-domain tunnel.

Additionally, oligopeptides of different sizes, including octapeptides, can inhibit PrfA-dependent gene expression.²⁶ While longer peptides may exert their effects when metabolically processed into smaller peptides, our PrfA-peptide structures suggest that peptides with more than four residues should also be able to directly inhibit PrfA. By superimposing the RGLL peptide bound in monomer B onto monomer A, we obtain a simple model of an artificial hexapeptide RGLLGR bound to PrfA (Figure 7A). Based on this model, we anticipate that in peptides equal to or longer than six amino acids, the centrally positioned hydrophobic residues would be buried in the tunnel and the terminal

residues would be exposed at both inter-domain tunnel entrances (Figures 7B and 7C). Whether the overhanging residues can modulate binding to PrfA by interacting with specific features at either entrance of the inter-domain tunnel remains to be determined.

The broad binding specificity of peptides to PrfA mirrors the sequence-independent peptide binding of the bacterial ABC oligopeptide transporters, to which the listerial Opp permease involved in the uptake of PrfA-activating and PrfA-inhibiting peptides belongs.²⁶ The peptide receptor subunit of these transporters—OppA and homologs such as AppA from *Bacillus* or DppA in gram-negative bacteria^{45–49}—shares striking similarities with PrfA in terms of binding mechanism. This is likely a consequence of convergent evolution toward broad specificity in peptide recognition. Thus, the bound peptide substrates in OppA are in β strand conformation, although in OppA they make main-chain contacts with the protein on both sides^{47,48,50} (Figures S6A and S6B). The bound peptides are also similarly buried in a cavity between two large receptor protein lobes, where water-filled hydrophobic pockets can readily accommodate diverse side chains imposing little binding specificity.^{28,50} At the same time, they preferentially bind to hydrophobic residues defining the peptide's binding register. The transported peptides also bind with similar affinity to the PrfA-inhibitory peptides. In addition, PrfA and the peptide receptor subunits of the oligopeptide transporters share the ability to bind to small di- and tripeptides.^{26,48–51}

The regulation of PrfA activity by small exogenous oligopeptides from the bacterial environment is reminiscent of the gram-positive quorum sensing mechanisms, involving Opp-transported (re-imported) peptide pheromones and short hydrophobic peptides.⁵² In these systems, small 5- to 8-residue signaling peptides bind with high specificity to transcription factors, the so-called

RRNPP family of peptide-sensing regulators.^{53,54} These interactions typically occur in deep inter-domain clefts and involve hydrogen bonding of the extended peptide backbone to the regulator. Specificity is conferred by non-bonded hydrophobic interactions and hydrogen bonds between the peptide side chains and the regulator.^{55–58} However, unlike PrfA, these interactions often lead to substantial conformational changes in the transcription factor—for example, from inactive monomeric to active multi-meric forms^{55–58}—and have binding affinities that are two orders of magnitude higher ($K_D \approx 0.1\text{--}0.5 \mu\text{M}$)^{55,59,60} compared to those of PrfA and its inhibitory peptides. The RRNPP regulators and now also the listerial virulence regulator PrfA are paradigmatic examples of how peptides mediate the control of transcription factor activity. RRNPP quorum-sensing signaling peptides can exhibit permissive recognition properties within a given regulator subfamily, enabling bacterial interspecies communication.^{59,61,62} PrfA is, however, unique in its very broad peptide-binding specificity. This non-specific peptide binding mechanism allows the facultative pathogen *L. monocytogenes* to utilize oligopeptides of diverse origins (animal, plant, microbial, and even self-derived), abundant in the bacterial habitat, to fine-tune the costly expression of its virulence factors.^{5,26}

Peptide-mediated PrfA regulation acts alongside other regulatory mechanisms that respond to different cues to effectively sense the environmental changes that signal the saprophyte-to-parasite transition of *L. monocytogenes*. In this role, PrfA functions like a metabolite multi-sensor, monitoring a spectrum of environmental cues such as sugars, fatty acids, GSH concentrations, redox states, pH, and oligopeptides.^{17,19–24,26} How these diverse cues crosstalk to coordinate the complex life cycle of *Listeria* outside and within a host remains to be elucidated.

Since PrfA activity is essential for the pathogenicity of *L. monocytogenes*, it is an obvious target for the development of anti-infectives. Previous studies identified a group of ring-fused 2-pyridone heterocycles that inhibit PrfA and reduce virulence factor expression in *L. monocytogenes*.^{34,35} Two groups on the 2-pyridone scaffold were found to be important for inhibition: a small hydrophobic group that binds to the PrfA tunnel site S1 and a second, larger hydrophobic group based on a naphthyl group that binds to site S2. Our study shows that these binding sites also play a significant role in peptide-mediated PrfA inhibition, indicating that peptides and ring-fused 2-pyridone inhibitors bind to the PrfA inter-domain tunnel in a similar manner despite their structural differences. The structural insights gained from the PrfA-peptide complexes presented here can guide the further development of anti-virulence precision anti-infectives targeting PrfA.

Limitations of the study

While our study presents high-resolution structures of the virulence regulator PrfA bound to different tri- and tetrapeptides, and a precise structural explanation of the mechanism of promiscuous (sequence-independent) oligopeptide inhibitory binding to PrfA, inclusion of a larger variety of peptides would have provided more detailed insight into the peptide features affecting binding affinity and the structural determinants involved. The use of longer peptides would have helped to pinpoint the size limitation for peptide accessibility and accommodation into the

inter-domain tunnel for effective PrfA inhibition. An aspect that remained unaddressed is the competitive binding of the PrfA-inhibiting peptides and the PrfA-activating cofactor GSH and the stoichiometry of the interaction. Another aspect that requires further characterization is whether there is potential negative cooperativity of peptide binding to the PrfA dimer, as well as experimentally documenting whether peptide binding to only one monomer suffices to inhibit PrfA.

RESOURCE AVAILABILITY

Lead contact

Further information and requests for resources and reagents should be directed to and will be fulfilled by the lead contact, Elisabeth Sauer-Eriksson (elisabeth.sauer-eriksson@umu.se).

Materials availability

All unique and stable reagents generated in this study are available upon request to the [lead contact](#) with a completed materials transfer agreement.

Data and code availability

- The crystal structures (atomic coordinates and structural factors) have been deposited in the Protein Data Bank (PDB, www.rcsb.org) and are publicly available as of the date of publication. Accession numbers are listed in the [key resources table](#).
- This paper does not report original code.
- Any additional information required to reanalyze the data reported in this paper is available from the [lead contact](#) upon request.

ACKNOWLEDGMENTS

A.E.S.-E. was funded by the Swedish Research Council (ID 2015-03607 and 2019-03771). In addition, funds are gratefully acknowledged from the Kempe Foundation and the Erling-Persson Family Foundation. Work at the J.A.V.-B. laboratory was supported by Wellcome (program grant no. WT074020MA), core Roslin Institute Strategic Program funding from the BBSRC (BB/J004227/1), and the Medical Research Council (grant no. MRC/IAA/014). We thank beamline staff at the European Synchrotron Radiation Facility (ESRF, France) and the Swiss Light Source (SLS, Switzerland) for support and access to beamlines ID23-2 and X06DA, respectively. We acknowledge MAX IV Laboratory and staff for time on Beamline Biomax under proposal 20180236. Research conducted at MAX IV, a Swedish national user facility, is supported by the Swedish Research Council under contract 2018-07152, the Swedish Governmental Agency for Innovation Systems under contract 2018-04969, and Formas under contract 2019-02496.

AUTHOR CONTRIBUTIONS

T.H., C.L., and A.E.S.-E. performed the X-ray crystallographic studies of PrfA-peptide complexes. C.G. purified the PrfA protein. M.S. and E.K. performed the *in vivo* PrfA inhibition screens and prepared the figures, and T.H. performed the DNA-binding-inhibition studies. J.A.V.-B. and A.E.S.-E. conceived the study, designed the research, acquired the funding, and, together with T.H., wrote the paper. All authors had editorial input on the final version of the manuscript.

DECLARATION OF INTERESTS

The authors declare no competing interests.

STAR★METHODS

Detailed methods are provided in the online version of this paper and include the following:

- [KEY RESOURCES TABLE](#)
- [METHOD DETAILS](#)

- Oligopeptides
- Screening of PrfA inhibitor peptides
- Protein purification
- Isothermal titration calorimetry (ITC)
- Bio-layer interferometry (BLI)
- Crystallization and data collection
- Processing, phasing and refinement
- QUANTIFICATION AND STATISTICAL ANALYSIS

SUPPLEMENTAL INFORMATION

Supplemental information can be found online at <https://doi.org/10.1016/j.celrep.2025.115290>.

Received: July 31, 2024

Revised: November 20, 2024

Accepted: January 17, 2025

Published: February 18, 2025

REFERENCES

1. Freitag, N.E., Port, G.C., and Miner, M.D. (2009). Listeria monocytogenes - from saprophyte to intracellular pathogen. *Nat. Rev. Microbiol.* 7, 623–628.
2. Radoshevich, L., and Cossart, P. (2018). Listeria monocytogenes: towards a complete picture of its physiology and pathogenesis. *Nat. Rev. Microbiol.* 16, 32–46.
3. Koopmans, M.M., Brouwer, M.C., Vazquez-Boland, J.A., and van de Beek, D. (2022). Human Listeriosis. *Clin. Microbiol. Rev.* 36, e0006019.
4. Sturm, A., Heinemann, M., Arnoldini, M., Benecke, A., Ackermann, M., Benz, M., Dormann, J., and Hardt, W.D. (2011). The cost of virulence: retarded growth of *Salmonella Typhimurium* cells expressing type III secretion system 1. *PLoS Pathog.* 7, e1002143.
5. Vasanthakrishnan, R.B., de Las Heras, A., Scortti, M., Deshayes, C., Colgrave, N., and Vázquez-Boland, J.A. (2015). PrfA regulation offsets the cost of Listeria virulence outside the host. *Environ. Microbiol.* 17, 4566–4579.
6. Tiensuu, T., Guerreiro, D.N., Oliveira, A.H., O'Byrne, C., and Johansson, J. (2019). Flick of a switch: regulatory mechanisms allowing Listeria monocytogenes to transition from a saprophyte to a killer. *Microbiology (Read.)* 165, 819–833.
7. Chakraborty, T., Leimeister-Wächter, M., Domann, E., Hartl, M., Goebel, W., Nichterlein, T., and Notermans, S. (1992). Coordinate regulation of virulence genes in Listeria monocytogenes requires the product of the prfA gene. *J. Bacteriol.* 174, 568–574.
8. Freitag, N.E., Rong, L., and Portnoy, D.A. (1993). Regulation of the prfA transcriptional activator of Listeria monocytogenes: multiple promoter elements contribute to intracellular growth and cell-to-cell spread. *Infect. Immun.* 61, 2537–2544.
9. Mengaud, J., Dramsi, S., Gouin, E., Vazquez-Boland, J.A., Milon, G., and Cossart, P. (1991). Pleiotropic control of Listeria monocytogenes virulence factors by a gene that is autoregulated. *Mol. Microbiol.* 5, 2273–2283.
10. Leimeister-Wächter, M., Haffner, C., Domann, E., Goebel, W., and Chakraborty, T. (1990). Identification of a gene that positively regulates expression of listeriolysin, the major virulence factor of listeria monocytogenes. *Proc. Natl. Acad. Sci. USA* 87, 8336–8340.
11. Hamon, M., Biernie, H., and Cossart, P. (2006). Listeria monocytogenes: a multifaceted model. *Nat. Rev. Microbiol.* 4, 423–434.
12. Scortti, M., Monzó, H.J., Lacharme-Lora, L., Lewis, D.A., and Vázquez-Boland, J.A. (2007). The PrfA virulence regulon. *Microb. Infect.* 9, 1196–1207.
13. de las Heras, A., Cain, R.J., Bielecka, M.K., and Vázquez-Boland, J.A. (2011). Regulation of Listeria virulence: PrfA master and commander. *Curr. Opin. Microbiol.* 14, 118–127.
14. Johansson, J., and Freitag, N.E. (2019). Regulation of Listeria monocytogenes Virulence. *Microbiol. Spectr.* 7.
15. Toledo-Arana, A., Dussurge, O., Nikitas, G., Sesto, N., Guet-Reville, H., Balestrino, D., Loh, E., Gripenland, J., Tiensuu, T., Vaitkevicius, K., et al. (2009). The Listeria transcriptional landscape from saprophytism to virulence. *Nature* 459, 950–956.
16. Johansson, J., Mandin, P., Renzoni, A., Chiaruttini, C., Springer, M., and Cossart, P. (2002). An RNA thermosensor controls expression of virulence genes in Listeria monocytogenes. *Cell* 110, 551–561.
17. Park, S.F., and Kroll, R.G. (1993). Expression of listeriolysin and phosphatidylinositol-specific phospholipase C is repressed by the plant-derived molecule cellobiose in Listeria monocytogenes. *Mol. Microbiol.* 8, 653–661.
18. Brehm, K., Ripio, M.T., Kretz, J., and Vázquez-Boland, J.A. (1999). The bvr locus of Listeria monocytogenes mediates virulence gene repression by beta-glucosides. *J. Bacteriol.* 181, 5024–5032.
19. Dos Santos, P.T., Thomasen, R.S.S., Green, M.S., Færgeman, N.J., and Kallipolitis, B.H. (2020). Free Fatty Acids Interfere with the DNA Binding Activity of the Virulence Regulator PrfA of Listeria monocytogenes. *J. Bacteriol.* 202, e00156-20.
20. Portman, J.L., Dubensky, S.B., Peterson, B.N., Whiteley, A.T., and Portnoy, D.A. (2017). Activation of the Listeria monocytogenes Virulence Program by a Reducing Environment. *mBio* 8, e01595-17.
21. Haber, A., Friedman, S., Lobel, L., Burg-Golani, T., Sigal, N., Rose, J., Livnat-Levanon, N., Lewinson, O., and Herskovits, A.A. (2017). L-glutamine Induces Expression of Listeria monocytogenes Virulence Genes. *PLoS Pathog.* 13, e1006161.
22. Lobel, L., Sigal, N., Borovok, I., Belitsky, B.R., Sonenshein, A.L., and Herskovits, A.A. (2015). The metabolic regulator CodY links Listeria monocytogenes metabolism to virulence by directly activating the virulence regulatory gene prfA. *Mol. Microbiol.* 95, 624–644.
23. Gaballa, A., Guariglia-Oropeza, V., Wiedmann, M., and Boor, K.J. (2019). Cross Talk between SigB and PrfA in Listeria monocytogenes Facilitates Transitions between Extra- and Intracellular Environments. *Microbiol. Mol. Biol. Rev.* 83, e00034-19.
24. Reniere, M.L., Whiteley, A.T., Hamilton, K.L., John, S.M., Lauer, P., Brennan, R.G., and Portnoy, D.A. (2015). Glutathione activates virulence gene expression of an intracellular pathogen. *Nature* 517, 170–173.
25. Gopal, S., Borovok, I., Ofer, A., Yanku, M., Cohen, G., Goebel, W., Kretz, J., and Aharonowitz, Y. (2005). A multidomain fusion protein in Listeria monocytogenes catalyzes the two primary activities for glutathione biosynthesis. *J. Bacteriol.* 187, 3839–3847.
26. Kryptou, E., Scortti, M., Grundström, C., Oelker, M., Luisi, B.F., Sauer-Eriksson, A.E., and Vázquez-Boland, J. (2019). Control of Bacterial Virulence through the Peptide Signature of the Habitat. *Cell Rep.* 26, 1815–1827.e5.
27. Vega, Y., Rauch, M., Banfield, M.J., Ermolaeva, S., Scortti, M., Goebel, W., and Vázquez-Boland, J.A. (2004). New Listeria monocytogenes prfA* mutants, transcriptional properties of PrfA* proteins and structure-function of the virulence regulator PrfA. *Mol. Microbiol.* 52, 1553–1565.
28. Eiting, M., Hagelüken, G., Schubert, W.D., and Heinz, D.W. (2005). The mutation G145S in PrfA, a key virulence regulator of Listeria monocytogenes, increases DNA-binding affinity by stabilizing the HTH motif. *Mol. Microbiol.* 56, 433–446.
29. Sheehan, B., Klarsfeld, A., Msadek, T., and Cossart, P. (1995). Differential activation of virulence gene expression by PrfA, the Listeria monocytogenes virulence regulator. *J. Bacteriol.* 177, 6469–6476.
30. Hall, M., Grundström, C., Begum, A., Lindberg, M.J., Sauer, U.H., Almqvist, F., Johansson, J., and Sauer-Eriksson, A.E. (2016). Structural basis for glutathione-mediated activation of the virulence regulatory protein PrfA in Listeria. *Proc. Natl. Acad. Sci. USA* 113, 14733–14738.
31. Berude, J.C., Kennouche, P., Reniere, M.L., and Portnoy, D.A. (2024). Listeria monocytogenes utilizes glutathione and limited inorganic sulfur

- compounds as sources of essential cysteine. *Infect. Immun.* 92, e0042223.
32. Brenner, M., Friedman, S., Haber, A., Livnat-Levanon, N., Borovok, I., Sigel, N., Lewinson, O., and Herskovits, A.A. (2022). Listeria monocytogenes TcyKLMN Cystine/Cysteine Transporter Facilitates Glutathione Synthesis and Virulence Gene Expression. *mBio* 13, e0044822.
 33. Liebschner, D., Afonine, P.V., Moriarty, N.W., Poon, B.K., Sobolev, O.V., Terwilliger, T.C., and Adams, P.D. (2017). Polder maps: improving OMIT maps by excluding bulk solvent. *Acta Crystallogr. D Struct. Biol.* 73, 148–157.
 34. Good, J.A.D., Andersson, C., Hansen, S., Wall, J., Krishnan, K.S., Begum, A., Grundström, C., Niemiec, M.S., Vaitkevicius, K., Chorell, E., et al. (2016). Attenuating Listeria monocytogenes Virulence by Targeting the Regulatory Protein PrfA. *Cell Chem. Biol.* 23, 404–414.
 35. Kulen, M., Lindgren, M., Hansen, S., Cairns, A.G., Grundström, C., Begum, A., van der Lingen, I., Bränström, K., Hall, M., Sauer, U.H., et al. (2018). Structure-Based Design of Inhibitors Targeting PrfA, the Master Virulence Regulator of Listeria monocytogenes. *J. Med. Chem.* 61, 4165–4175.
 36. Stanfield, R.L., and Wilson, I.A. (1995). Protein-peptide interactions. *Curr. Opin. Struct. Biol.* 5, 103–113.
 37. Pawson, T., and Nash, P. (2003). Assembly of cell regulatory systems through protein interaction domains. *Science* 300, 445–452.
 38. London, N., Movshovitz-Attias, D., and Schueler-Furman, O. (2010). The structural basis of peptide-protein binding strategies. *Structure* 18, 188–199.
 39. Rodgers, T.L., Townsend, P.D., Burnell, D., Jones, M.L., Richards, S.A., McLeish, T.C.B., Pohl, E., Wilson, M.R., and Cann, M.J. (2013). Modulation of global low-frequency motions underlies allosteric regulation: demonstration in CRP/FNR family transcription factors. *PLoS Biol.* 11, e1001651.
 40. Eisen, H.N., Hou, X.H., Shen, C., Wang, K., Tanguturi, V.K., Smith, C., Kozyrytska, K., Nambiar, L., McKinley, C.A., Chen, J., and Cohen, R.J. (2012). Promiscuous binding of extracellular peptides to cell surface class I MHC protein. *Proc. Natl. Acad. Sci. USA* 109, 4580–4585.
 41. Bhattacharjee, A., and Wallin, S. (2013). Exploring Protein-Peptide Binding Specificity through Computational Peptide Screening. *PLoS Comput. Biol.* 9, e1003277.
 42. Vanhee, P., Stricher, F., Baeten, L., Verschueren, E., Lenaerts, T., Serrano, L., Rousseau, F., and Schymkowitz, J. (2009). Protein-peptide interactions adopt the same structural motifs as monomeric protein folds. *Structure* 17, 1128–1136.
 43. Nguyen, H.Q., Roy, J., Harink, B., Damle, N.P., Latorraca, N.R., Baxter, B.C., Brower, K., Longwell, S.A., Kortemme, T., Thorn, K.S., et al. (2019). Quantitative mapping of protein-peptide affinity landscapes using spectrally encoded beads. *Elife* 8, e40499.
 44. Parker, B.W., Goncz, E.J., Krist, D.T., Statsyuk, A.V., Nesvizhskii, A.I., and Weiss, E.L. (2019). Mapping low-affinity/high-specificity peptide-protein interactions using ligand-footprinting mass spectrometry. *Proc. Natl. Acad. Sci. USA* 116, 21001–21011.
 45. Monnet, V. (2003). Bacterial oligopeptide-binding proteins. *Cell. Mol. Life Sci.* 60, 2100–2114.
 46. Tame, J.R., Murshudov, G.N., Dodson, E.J., Neil, T.K., Dodson, G.G., Higgins, C.F., and Wilkinson, A.J. (1994). The structural basis of sequence-independent peptide binding by OppA protein. *Science* 264, 1578–1581.
 47. Dunten, P., and Mowbray, S.L. (1995). Crystal structure of the dipeptide binding protein from *Escherichia coli* involved in active transport and chemotaxis. *Protein Sci.* 4, 2327–2334.
 48. Berntsson, R.P.A., Doeven, M.K., Fusetti, F., Duurkens, R.H., Sengupta, D., Marinik, S.J., Thunnissen, A.M.W.H., Poolman, B., and Slotboom, D.J. (2009). The structural basis for peptide selection by the transport receptor OppA. *EMBO J.* 28, 1332–1340.
 49. Levdikov, V.M., Blagova, E.V., Brannigan, J.A., Wright, L., Vagin, A.A., and Wilkinson, A.J. (2005). The structure of the oligopeptide-binding protein, AppA, from *Bacillus subtilis* in complex with a nonapeptide. *J. Mol. Biol.* 345, 879–892.
 50. Tame, J.R., Dodson, E.J., Murshudov, G., Higgins, C.F., and Wilkinson, A.J. (1995). The crystal structures of the oligopeptide-binding protein OppA complexed with tripeptide and tetrapeptide ligands. *Structure* 3, 1395–1406.
 51. Berntsson, R.P.A., Thunnissen, A.M.W.H., Poolman, B., and Slotboom, D.J. (2011). Importance of a hydrophobic pocket for peptide binding in lacticoccal OppA. *J. Bacteriol.* 193, 4254–4256.
 52. Slamti, L., and Lereclus, D. (2019). The oligopeptide ABC-importers are essential communication channels in Gram-positive bacteria. *Res. Microbiol.* 170, 338–344.
 53. Rocha-Estrada, J., Aceves-Diez, A.E., Guarneros, G., and de la Torre, M. (2010). The RNPP family of quorum-sensing proteins in Gram-positive bacteria. *Appl. Microbiol. Biotechnol.* 87, 913–923.
 54. Declerck, N., Bouillaud, L., Chaix, D., Rugani, N., Slamti, L., Hoh, F., Lereclus, D., and Arold, S.T. (2007). Structure of PlcR: Insights into virulence regulation and evolution of quorum sensing in Gram-positive bacteria. *Proc. Natl. Acad. Sci. USA* 104, 18490–18495.
 55. Zouhir, S., Perchat, S., Nicaise, M., Perez, J., Guimaraes, B., Lereclus, D., and Nessler, S. (2013). Peptide-binding dependent conformational changes regulate the transcriptional activity of the quorum-sensor NprR. *Nucleic Acids Res.* 41, 7920–7933.
 56. Talagas, A., Fontaine, L., Ledesma-García, L., Mignolet, J., Li de la Sierra-Gallay, I., Lazar, N., Aumont-Nicaise, M., Federle, M.J., Prehna, G., Hols, P., and Nessler, S. (2016). Structural Insights into Streptococcal Competence Regulation by the Cell-to-Cell Communication System ComRS. *PLoS Pathog.* 12, e1005980.
 57. Neiditch, M.B., Capodagli, G.C., Prehna, G., and Federle, M.J. (2017). Genetic and Structural Analyses of RRNPP Intercellular Peptide Signaling of Gram-Positive Bacteria. *Annu. Rev. Genet.* 51, 311–333.
 58. Do, H., and Kumaraswami, M. (2016). Structural Mechanisms of Peptide Recognition and Allosteric Modulation of Gene Regulation by the RRNPP Family of Quorum-Sensing Regulators. *J. Mol. Biol.* 428, 2793–2804.
 59. Shanker, E., Morrison, D.A., Talagas, A., Nessler, S., Federle, M.J., and Prehna, G. (2016). Pheromone Recognition and Selectivity by ComR Proteins among Streptococcus Species. *PLoS Pathog.* 12, e1005979.
 60. Aggarwal, C., Jimenez, J.C., Nanavati, D., and Federle, M.J. (2014). Multiple length peptide-pheromone variants produced by *Streptococcus pyogenes* directly bind Rgg proteins to confer transcriptional regulation. *J. Biol. Chem.* 289, 22427–22436.
 61. Fleuchot, B., Guillot, A., Mézange, C., Basset, C., Chambellan, E., Monnet, V., and Gardan, R. (2013). Rgg-associated SHP signaling peptides mediate cross-talk in Streptococci. *PLoS One* 8, e66042.
 62. Cook, L.C., and Federle, M.J. (2014). Peptide pheromone signaling in *Streptococcus* and *Enterococcus*. *FEMS Microbiol. Rev.* 38, 473–492.
 63. Winn, M.D., Ballard, C.C., Cowtan, K.D., Dodson, E.J., Emsley, P., Evans, P.R., Keegan, R.M., Krissinel, E.B., Leslie, A.G.W., McCoy, A., et al. (2011). Overview of the CCP4 suite and current developments. *Acta Crystallogr. D Biol. Crystallogr.* 67, 235–242.
 64. Liebschner, D., Afonine, P.V., Baker, M.L., Bunkóczki, G., Chen, V.B., Croll, T.I., Hintze, B., Hung, L.W., Jain, S., McCoy, A.J., et al. (2019). Macromolecular structure determination using X-rays, neutrons and electrons: recent developments in Phenix. *Acta Crystallogr. D Struct. Biol.* 75, 861–877.
 65. Emsley, P., Lohkamp, B., Scott, W.G., and Cowtan, K. (2010). Features and development of Coot. *Acta Crystallogr. D Biol. Crystallogr.* 66, 486–501.
 66. McNicholas, S., Potterton, E., Wilson, K.S., and Noble, M.E.M. (2011). Presenting your structures: the CCP4mg molecular-graphics software. *Acta Crystallogr. D Biol. Crystallogr.* 67, 386–394.

67. Stourac, J., Vavra, O., Kokkonen, P., Filipovic, J., Pinto, G., Brezovsky, J., Damborsky, J., and Bednar, D. (2019). Caver Web 1.0: identification of tunnels and channels in proteins and analysis of ligand transport. *Nucleic Acids Res.* **47**, W414–W422.
68. Kabsch, W. (2010). XDS. *Acta Crystallogr. D Biol. Crystallogr.* **66**, 125–132.
69. Evans, P.R., and Murshudov, G.N. (2013). How good are my data and what is the resolution? *Acta Crystallogr. D Biol. Crystallogr.* **69**, 1204–1214.
70. McCoy, A.J., Grosse-Kunstleve, R.W., Adams, P.D., Winn, M.D., Storoni, L.C., and Read, R.J. (2007). Phaser crystallographic software. *J. Appl. Crystallogr.* **40**, 658–674.
71. Afonine, P.V., Grosse-Kunstleve, R.W., Echols, N., Headd, J.J., Moriarty, N.W., Mustyakimov, M., Terwilliger, T.C., Urzhumtsev, A., Zwart, P.H., and Adams, P.D. (2012). Towards automated crystallographic structure refinement with phenix.refine. *Acta Crystallogr. D Biol. Crystallogr.* **68**, 352–367.
72. Terwilliger, T.C., Klei, H., Adams, P.D., Moriarty, N.W., and Cohn, J.D. (2006). Automated ligand fitting by core-fragment fitting and extension into density. *Acta Crystallogr. D Biol. Crystallogr.* **62**, 915–922.
73. Terwilliger, T.C., Adams, P.D., Moriarty, N.W., and Cohn, J.D. (2007). Ligand identification using electron-density map correlations. *Acta Crystallogr. D Biol. Crystallogr.* **63**, 101–107.

STAR★METHODS

KEY RESOURCES TABLE

REAGENT or RESOURCE	SOURCE	IDENTIFIER
Bacterial and virus strains		
<i>Listeria monocytogenes</i> P14-P _{hly-lux}	Our laboratory	N/A
<i>Escherichia coli</i> BI21(DE3)- Novagen	Our laboratory	N/A
Chemicals, peptides, and recombinant proteins		
Custom peptides (>90% purity, TFA-salt) LL, LLL, EVF, EVFL, STLL, RGLL, TKPR, TEPL, LIVA	GenScript	N/A
Custom peptides (>95% purity, acetate-salt) EVF, EVFL, STLL, RGLL, TKPR, TEPL	GenScript	N/A
LL peptide (>98% purity)	Sigma-Aldrich	Cat#L2752
LLL peptide (>90% purity)	Sigma-Aldrich	Cat#L0879
EVF peptide (>98% purity)	Sigma-Aldrich	Cat#G3751
AG peptide (>99% purity)	Sigma-Aldrich	Cat#A0878
Glutathione (GSH) reduced	Sigma-Aldrich	Cat#G-4251
PrfA wild type	Our laboratory	N/A
Deposited data		
Model of PrfA-GSH	Hall et al. ³⁰	PDB ID: 5lrr
Model of PrfA-LL	Krypotou et al. ²⁶	PDB ID: 6hck
Model of PrfA-LLL	This study	PDB ID: 8cb4
Model of PrfA-EVF	This study	PDB ID: 8cb5
Model of PrfA-EVFL	This study	PDB ID: 8cb7
Model of PrfA-STLL	This study	PDB ID: 8cb8
Model of PrfA-RGLL	This study	PDB ID: 8cbg
Model of PrfA-TKPR	This study	PDB ID: 8cbi
Model of PrfA-TEPL	This study	PDB ID: 8cbp
Oligonucleotides		
<i>plcA/hly</i> PrfA box biotinylated oligonucleotides	Eurofins Genomics	https://eurofinsgenomics.eu/
Recombinant DNA		
pet28a-6His-TEV-PrfA	Our laboratory	N/A
Software and algorithms		
Origin 7.0	OriginLab	https://www.originlab.com/
Octet Analysis Studio software	Sartorius	https://www.sartorius.com/
Mars Data Analysis Software	BMG	https://www.bmglabtech.com/
Prism 10.3.0 for macOS	GraphPad Software LLC	https://www.graphpad.com/
CCP4 software suite	Winn et al. ⁶³	https://www.ccp4.ac.uk/
PHENIX program suite	Liebschner et al. ⁶⁴	https://phenix-online.org/
COOT	Emsley et al. ⁶⁵	https://www2.mrc-lmb.cam.ac.uk/personal/pemsley/coot/
ICM Browser	Molsoft LLC	https://www.molsoft.com/icm_browser.html
CCP4mg	McNicholas et al. ⁶⁶	https://www.ccp4.ac.uk/MG/
Caver Web	Stourac et al. ⁶⁷	https://loschmidt.chemi.muni.cz/caverweb/

METHOD DETAILS

Oligopeptides

Three independent batches of lyophilized oligopeptides with verified masses were purchased from Sigma-Aldrich (one batch) and GenScript (two batches). For *in vivo* PrfA inhibition studies, oligopeptides were dissolved at 8 mM in sterile pure water and aliquoted in single-use vials at -20°C. For ITC/BLI assays, oligopeptides were dissolved in water to a final concentration of 10 mM, aliquoted

and stored at -20°C . The aliquots were thawed and used immediately for the ITC/BLI assays. The BLI assays performed with all three batches gave identical results. For crystallization, the oligopeptides were dissolved in DMSO to a final concentration of 50 or 100 mM.

Screening of PrfA inhibitor peptides

PrfA *in vivo* inhibition studies used *L. monocytogenes* P14-P_{hly-lux}, a wild-type serovar 4b isolate carrying a chromosomally integrated *luxABCDE* reporter under the control of the PrfA-regulated *hly* promoter.²⁶ Bacterial cultures were prepared in BHI broth (BD-Difco) supplemented with 7.5 µg/mL chloramphenicol and incubated overnight at 37°C . Cultures were washed, resuspended in PBS and used to inoculate fresh PrfA-activating chemically defined medium (CDM) to an initial optical density at 600 nm (OD₆₀₀) of 0.02–0.05. Duplicate 200-µL aliquots were transferred to opaque 96-well plates with clear optical bottoms (ThermoScientific), and OD₆₀₀ and luminescence readings were taken every 30 min during incubation in an automated microplate reader (FLUOstar Omega, BMG Labtech). The bioluminescence values were normalized to growth at each time point by dividing the luminescence readings by the OD₆₀₀.

Peptides were added to CDM medium to a final concentration of 1 mM.²⁶ CDM composition: 6.56 g/L KH₂OP₄, 30.96 g/L Na₂HPO₄·7H₂O, 0.41 g/L MgSO₄, 88 mg/L ferric citrate, 0.1 g/L each of the (L-) amino acids leucine, isoleucine, valine, methionine, arginine, cysteine, histidine, and tryptophan, 0.6 g/L L-glutamine, 2.5 mg/L adenine, 0.5 mg/L biotin, 5 mg/L riboflavin, 1 mg/L each of thiamine, pyridoxal, *para*-aminobenzoic acid, calcium pantothenate, and nicotinamide, 5 µg/L thioctic acid, and 4.5 g/L glucose. CDM was freshly prepared from filter-sterilized stock solutions from each of the components stored at 4°C (with the exception of glutamine, biotin and ferric citrate solutions, which were stored at -20°C ; phosphates, MgSO₄ and glucose, stored at room temperature; and cysteine, which was freshly prepared).

Protein purification

PrfA^{WT} was recombinantly expressed in *E. coli* BL21(DE3) using a pET28a plasmid with a 6-His tag and a TEV (tobacco etch virus) cleavage site. Overnight cultures of the transformed strain in LB medium were diluted 1:100 and grown at 37°C to an OD₆₀₀ of 0.4–0.6. The temperature was then lowered to 18°C and PrfA expression was induced with 0.5 mM isopropyl β-d-1-thiogalactopyranoside (IPTG). Cells were cultured at 18°C for ~16 h before harvesting. After sonication, PrfA was purified from the supernatant using Ni-NTA (Qiagen). After elution with imidazole, PrfA was incubated with TEV protease (100:1 M ratio) for ~12 h at 4°C in imidazole-free buffer to remove the 6-His tag. The cleaved protein was reloaded onto Ni-NTA, and the flow-through contained full-length PrfA with two additional N-terminal residues (GA) from the cleavage site. The protein was further purified on a MonoS 10/10 ion-exchange column, eluting at 250 mM NaCl in 10 mM Tris pH 7.5 followed by size-exclusion chromatography on a HiLoad Superdex 75 16/60 column in 20 mM sodium phosphate pH 6.5, 200 mM NaCl. The PrfA fractions were pooled and concentrated using a Centri-prep-10 centrifugal concentrator (Millipore).

Isothermal titration calorimetry (ITC)

PrfA and oligopeptides were prepared in a buffer containing 20 mM Tris-HCl pH 8 and 200 mM NaCl. In the calorimetry experiments, 50 µM PrfA was titrated against 0.5 mM or 2 mM oligopeptides. The experiments were performed at 25°C using a MicroCal auto-ITC200 calorimeter (MicroCal-Malvern) and the standard methods “Plates Prerinse Syringe Clean” and “EDTA”. After subtracting the isotherms obtained by injecting oligopeptides into the buffer alone, the binding isotherms were fitted to the “one set of sites” model implemented in Origin 7 (OriginLab). The experiments were performed in independent triplicates. The binding affinities of peptides TKPR and TEPL could not be determined, as their interactions with PrfA appear too weak to be detected under the experimental conditions. Increasing PrfA concentrations caused solubility problems, while higher peptide concentrations generated excessive background heat, preventing accurate measurements.

Bio-layer interferometry (BLI)

The binding and dissociation of PrfA to DNA was measured in real time using an Octet system (Sartorius) using a 50-mer double-stranded biotinylated DNA probe containing the *plcA/hly* PrfA box.²⁶ The probe was prepared by heating a 1:1.1 mixture of the 5'-biotinylated oligonucleotide 5'-[BIOTEG]TGTCCCTTATCGCTGTTAACAAATGTTAATGCCTCGACA-3' and the non-biotinylated complementary DNA oligonucleotide 5'-TGTCGAGGCATTAACATTGTTAACGACGATAAAGGGACA-3' in boiling water followed by slow cooling for annealing. 100 nM dsDNA was captured on streptavidin (SA) biosensors and incubated at 25°C with a shaking speed of 1000 rpm in a buffer containing 50 mM Tris-HCl pH 7.5, 300 mM NaCl, and 0.05% Tween 20. The biosensors were incubated in a 2-fold dilution series of PrfA-oligopeptide mixtures (1:100 M ratio) and a PrfA-GSH mixture (GSH maintained at 5 mM) in the same buffer. The times for the baseline, association, and dissociation steps were 180, 300, and 600 s, respectively. After subtracting the control and reference sensor signals, the sensorgrams were analyzed using the Octet Analysis Studio software (Sartorius) to determine the binding responses.

Crystallization and data collection

For co-crystallization, 3.1–6.6 mg mL⁻¹ PrfA in 20 mM sodium phosphate at pH 6.5, 200 mM NaCl was mixed with the peptides and dithiothreitol (DTT) to obtain a 1:10 M ratio of protein to peptide and final concentrations of 0.5–2.5 mM peptides, 0.5–2.5% (v/v) DMSO and 1–4 mM DTT. The mixture was incubated for 4 to 14 h at room temperature or 4°C prior to crystallization. Crystallization was performed by the hanging-drop or sitting-drop vapor diffusion method at 18°C . For this purpose, the protein-peptide mixture

was mixed in a 1:1 ratio with the crystallization solution containing 100 mM sodium citrate with a pH of 5.1–5.7, 16% (w/v) to 26% (w/v) PEG4000, and 0% (v/v) or 17% (v/v) isopropanol. All crystals, except the PrfA-tri-leucine crystal (PrfA-LLL), were additionally soaked with 20 mM peptides, 35% (w/v) PEG4000 and 100 mM sodium citrate before vitrification in liquid nitrogen. The cryoprotection solution consisted of the crystallization condition and an increased PEG4000 concentration of 35% (w/v). The exact crystallization conditions are given in the Protein DataBank for each PrfA-peptide complex. Data collection was performed at 100 K at synchrotrons specified in [Table S1](#).

Processing, phasing and refinement

The diffraction images were processed with XDS⁶⁸ and scaled and merged using AIMLESS from the CCP4 software suite.^{63,69} The structure was determined by molecular replacement with the PHASER program from the PHENIX program suite^{64,70} using the wild-type PrfA-di-leucine complex structure (PrfA-LL, PDB code 6hck²⁶) as a search model. The atomic models were manually built using COOT⁶⁵ and refined with PHENIX Refine.⁷¹ Noncrystallographic symmetry restraints were not applied during refinement. The quality of the electron density map of the ligand was significantly improved in the POLDER omit map,³³ and the ligand was modeled with the aid of LigandFit.^{72,73} The turns within the HTH motifs were flexible and could not be modeled for all structures (~residues Gly175-His182). In addition, the C-terminal DNA binding domain was poorly defined in the electron density of monomer A of the PrfA-TEPL complex structures, meaning residues Val198–Val208 could not be modeled. Only peptide residues defined in the electron density were included in the final model. For residue Glu2 in the TEPL peptide, the position of its side chain was not defined in the electron density. Refinement statistics are shown in [Table S1](#). Structural figures were prepared with CCP4mg,⁶⁶ ICM Browser (Molsoft LLC), and CAVER Web.⁶⁷ The electrostatic charge distribution in [Figure 3E](#) was prepared with CCP4mg.⁶⁶

QUANTIFICATION AND STATISTICAL ANALYSIS

The statistical analyses were carried out using Prism software (version 10, GraphPad). The figure legends include the exact number of replicates for each experiment and the specific statistical analysis.